Appl. Phys. B 73, 383–390 (2001)
DOI: 10.1007/s003400100648

Applied Physics B
Lasers and Optics

N. DEL FATTI
F. VALLÉE✉

Ultrafast optical nonlinear properties of metal nanoparticles

CPMOH, CNRS – Université Bordeaux I, 351 cours de la Libération, 33405 Talence, France

Received: 4 July 2001
Published online: 10 October 2001 •

ABSTRACT The physical origin and the dynamics of the ultrafast optical nonlinear response of noble metal nanoparticles are analyzed around the surface plasmon resonance frequency using extension of the bulk metal electron kinetics and band structure models. The computed spectral and temporal responses are found to be in very good agreement with the measured ones in silver when taking into account the impact of electron excitation on both the interband absorption and electron optical scattering rate. A good reproduction of the strong excitation regime experimental results is also obtained in the case of gold, with a dominant contribution of the interband effect.

PACS 78.47.+p; 42.65.-k; 73.20.Mf

1 Introduction

The most conspicuous manifestation of confinement in the optical properties of metal nanoparticles is the appearance of a morphological resonance, the surface plasmon resonance (SPR), that strongly enhances their linear and nonlinear responses around specific wavelengths [1–5]. This resonance is a direct consequence of dielectric confinement (i.e., of the local field effect) and, in an elementary classical model, can be interpreted in terms of a collective motion of the electrons in a nanoparticle. In the case of alkaline and noble metals, the SPR shows up as a well-defined resonance in the material absorption, with spectral characteristics determined by the conduction and core electron properties in the confined medium [1, 2].

The impact of dielectric confinement on the nonlinear optical response of metal nanoparticles has been extensively studied using different techniques on different time scales, demonstrating its resonant enhancement in the vicinity of the SPR [3–6]. Only recently has this response been investigated on time scales of a few hundreds or even a few tens of femtoseconds, using time-resolved pump-probe techniques [6–15]. These have the advantage of permitting a time domain separation of the different contributions of the electrons and lattice to the nonlinear response, and thus a precise determination of its physical origin in nanometric size materials. In particular, it has been shown that, in addition to the electronic bulk-like nonlinear processes, new nonlinear electronic mechanisms take place in nanoparticles, associated with electronic quantum confinement [6, 12].

In this paper we discuss the ultrafast optical nonlinearity around the SPR and its connection with the ultrafast electron dynamics in relatively large metal nanoparticles (radii larger than typically 5 nm) whose spectral and dynamic properties can be conveniently described using a small-solid approach. We will focus here on the modification of the bulk-like response by confinement, discussing mostly the interband contribution to the nonlinear response of noble metals (Ag and Au), which are considered to be model systems. The results of theoretical modeling, based on extensions of our studies in bulk noble metals [16], are quantitatively compared to the experimental data obtained in silver nanoparticles, using sub-30 fs pulses in the weak perturbation regime [6, 12], and in gold nanoparticles for strong excitations [10].

2 Linear optical properties of metal nanoparticles

The linear properties of a composite material formed by nanoparticles dispersed in a liquid or solid matrix can be described by introducing an effective dielectric function, $\widetilde{\varepsilon}$. For a low volume fraction $p \ll 1$ of small spheres ($R \ll \lambda$, where λ is the optical wavelength), it is given by [1–3]:

$$\widetilde{\varepsilon}(\omega) = \varepsilon_\mathrm{d} + 3p\varepsilon_\mathrm{d}\frac{\varepsilon(\omega)-\varepsilon_\mathrm{d}}{\varepsilon(\omega)+2\varepsilon_\mathrm{d}}\,, \tag{1}$$

where ε and ε_d are the dielectric constants of the metal nanoparticle and matrix, respectively. The latter will be assumed to be frequency independent and real in the spectral range of interest. The absorption coefficient of the composite material then can be written as follows [1, 2, 4]:

$$\widetilde{\alpha}(\omega) = \frac{9p\varepsilon_\mathrm{d}^{3/2}}{c}\frac{\omega\,\varepsilon_2(\omega)}{[\varepsilon_1(\omega)+2\varepsilon_\mathrm{d}]^2+\varepsilon_2^2(\omega)}\,, \tag{2}$$

where $\varepsilon(\omega) = \varepsilon_1(\omega) + \mathrm{i}\varepsilon_2(\omega)$. As compared to the bulk metal, absorption is resonantly enhanced close to the frequency, Ω_R, minimizing the denominator which is the condition for surface plasmon resonance (SPR). This is concomitant with enhancement of the electric field inside the particle as compared

✉ Fax: +33/05-5684-6970, E-mail: fvallee@cribx1.u-bordeaux.fr

to the applied field and can be described in terms of a local field effect [2–4]. The same effect is responsible for the enhancement of the nonlinear response, whose physical origin can be traced back to the electron distribution dependence of the metal dielectric constant.

In bulk noble metals, the conduction electrons follow a quasi-free electron behavior, and their contribution to the dielectric constant at the frequency ω is well described by a Drude formula [17]:

$$\varepsilon^{\mathrm{f}}(\omega) = 1 - \frac{\omega_{\mathrm{p}}^2}{\omega[\omega + \mathrm{i}/\tau_{\mathrm{o}}(\omega)]}\,, \tag{3}$$

where ω_{p} is the plasma frequency ($\omega_{\mathrm{p}}^2 = n_{\mathrm{e}}\mathrm{e}^2/\varepsilon_0 m$). $\tau_{\mathrm{o}}(\omega)$ is the electron optical relaxation time, which is determined by electron–phonon and electron–electron scattering with simultaneous exchange of the energy $\hbar\omega$ of a photon, and leads to intraband (free electron) absorption. The presence of the bound electrons leads to an additional contribution to ε so that the complete dielectric constant is [18]:

$$\varepsilon(\omega) = \varepsilon^{\mathrm{f}}(\omega) + \delta\varepsilon^{\mathrm{b}}(\omega)\,, \tag{4}$$

where $\delta\varepsilon^{\mathrm{b}} = \varepsilon^{\mathrm{b}} - 1$. The quasi-free electron response is modified in a nanocrystal by electron interaction with the interface, and one can show that the intraband contribution to ε preserves its Drude form (3), with the scattering time now being [1–3, 12, 19]

$$\frac{1}{\tau(\omega)} = \frac{1}{\tau_{\mathrm{o}}'(\omega)} + g_{\mathrm{S}}\frac{V_{\mathrm{F}}}{R}\,, \tag{5}$$

where τ_{o}' reflects bulk-like electron scattering in the particle, V_{F} is the Fermi velocity and g_{S} is an electron-distribution-dependent proportionality factor [2, 19]. The second term is a consequence of electron confinement, and classically, it can be ascribed to electron scattering off the surface. In a more correct quantum mechanical description, it is a consequence of modification of the electron wave functions and is thus a manifestation of quantum confinement in the optical response.

For not too small particles ($R \geq 1.5$ nm), modification of the interband transition spectrum can be neglected [20]. The nanocrystallite dielectric constant can thus be obtained by using the measured bulk metal dielectric constant [17] and introducing the surface correction as a parameter to reproduce

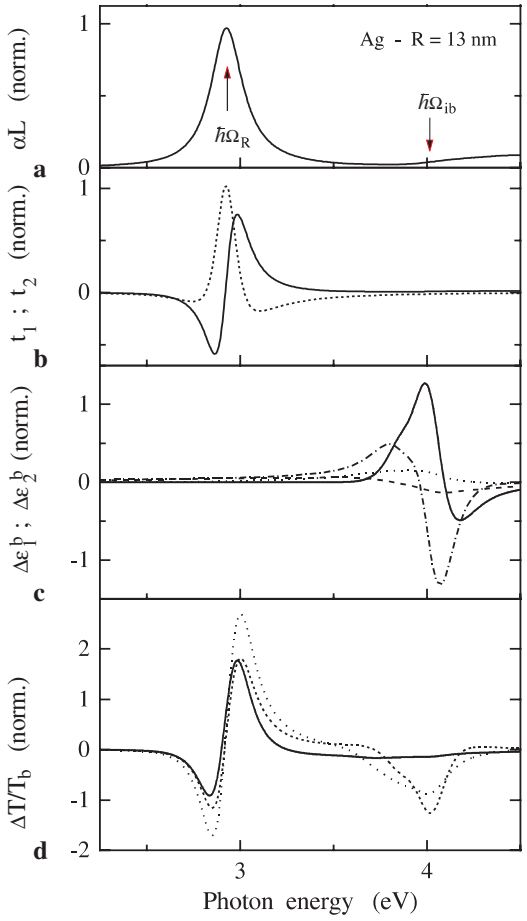

FIGURE 1 **a** Fit to the measured absorption spectra of $R = 13$ nm silver nanoparticles in glass. The SPR frequency ($\hbar\Omega_{\mathrm{R}} = 2.93$ eV) and interband transition threshold ($\hbar\Omega_{\mathrm{ib}}$) are indicated. **b** Dispersion of the coefficients t_1 (*solid line*) and t_2 (*dashed line*) linking $\Delta T/T$ to $\Delta\varepsilon_1$ and $\Delta\varepsilon_2$ (6) for the same sample. **c** Interband contribution to $\Delta\varepsilon_1$ and $\Delta\varepsilon_2$ calculated for $t_{\mathrm{D}} = 0$ fs (*dashed and dotted lines*) and $t_{\mathrm{D}} = 500$ fs (*dash-dotted and solid lines*) for excitation with a 25 fs near-infrared pulse and $\Delta T_{\mathrm{e}}^{\mathrm{me}} = 100$ K. **d** Corresponding transmission change due to the interband contribution for $t_{\mathrm{D}} = 0$, 100 and 500 fs (*solid, dotted and dashed lines*, respectively)

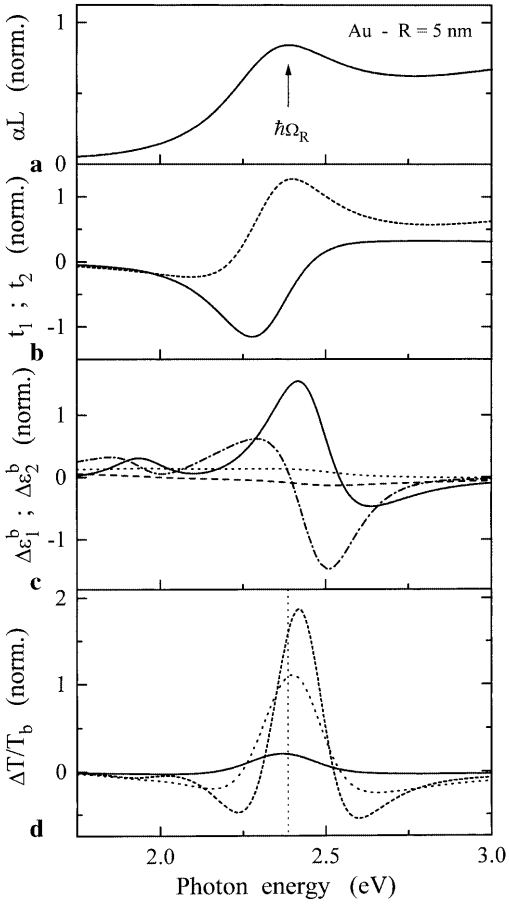

FIGURE 2 Same as Fig. 1, but for $R = 5$ nm gold nanoparticles in solution. The low- and high-energy structures in **c** are due to the X and L point contributions, respectively. The *line* in **d** indicates the SPR frequency $\hbar\Omega_R = 2.39$ eV

the measured absorption spectra [6]. The deduced expression of ε will be used in the following to discuss the nanoparticles nonlinear optical properties.

Because of the large frequency threshold for the interband transitions in silver ($\hbar\Omega_{\rm ib} \approx 4$ eV), the SPR lies in an isolated region of the spectrum and shows up as a well-defined resonance (Fig. 1). This is in contrast to other metals, for which the SPR overlaps the interband transitions, as shown for gold colloid in Fig. 2. In the following we will discuss the influence of this overlap on the nonlinear response of metal nanoparticles using silver and gold as model systems.

3 Nonlinear optical properties of metal nanoparticles

The time-dependent alteration of the dielectric constant of a material by a femtosecond pulse, i.e., its ultrafast nonlinear optical response can be investigated by monitoring its optical properties (transmission, T, and/or reflectivity, R) using a delayed probe pulse. If the perturbation is sufficiently weak, a perturbational approach can be used. In a dilute composite material, the normalized transmission change $\Delta T/T(\omega_{\rm pr}, t_{\rm D})$ at the probe frequency $\omega_{\rm pr}$ is only determined by $\Delta\widetilde{\varepsilon}_2(\omega_{\rm pr}, t_{\rm D})$, or, equivalently, by the sample absorption change [6]:

$$\Delta T/T = -\Delta\widetilde{\alpha}L = t_1\Delta\varepsilon_1 + t_2\Delta\varepsilon_2 \,, \tag{6}$$

where L is the sample thickness and $t_{\rm D}$ the pump–probe delay. t_1 and t_2 are entirely determined using (2) and $\varepsilon(\omega_{\rm pr})$ in the nanoparticles (Figs. 1 and 2).

To analyze the physical origin of the ultrafast nonlinear response, one has to connect $\Delta\varepsilon$ to the electron and lattice property changes. ε depends on the transient electron distribution in the different bands. Here we will only discuss effects associated with the conduction electron distribution change, Δf, assuming that only intraband conduction band absorption of the pump pulse takes place. This assumption is not very restrictive in noble metals, since when interband absorption takes place the created d-band holes recombine in a few tens of femtoseconds, the absorbed energy being transferred to the conduction electrons [21, 22]. Except for the few first tens of femtoseconds, the electron dynamics will thus be very similar for intra and interband absorptions, leading to similar transient optical property changes.

Intraband absorption of a femtosecond pulse of frequency $\omega_{\rm pp}$ leads to the creation of a strongly athermal electron distribution [6, 16, 23, 24], electrons with an energy E between $E_{\rm F} - \hbar\omega_{\rm pp}$ and $E_{\rm F}$ being excited above the Fermi energy with a final energy between $E_{\rm F}$ and $E_{\rm F} + \hbar\omega_{\rm pp}$ (Fig. 3). Electron–electron scattering redistributes the energy in the electron gas, eventually leading to a hot Fermi distribution with temperature, $T_{\rm e}$ (the characteristic thermalization times are ≈ 500 fs and 350 fs in bulk Au and Ag, respectively [16, 23]). During and after internal thermalization, energy is transferred to the lattice by electron–phonon interactions, with a characteristic time of typically 1 ps. This energy redistribution kinetics has been modeled numerically by solving the electron Boltzmann equation [16, 23]. The electron distribution changes computed in bulk silver for a pump photon energy $\hbar\omega_{\rm pp} = 1.3$ eV and 25 fs pulse duration are shown in Fig. 3, for $t_{\rm D} = 0$ and

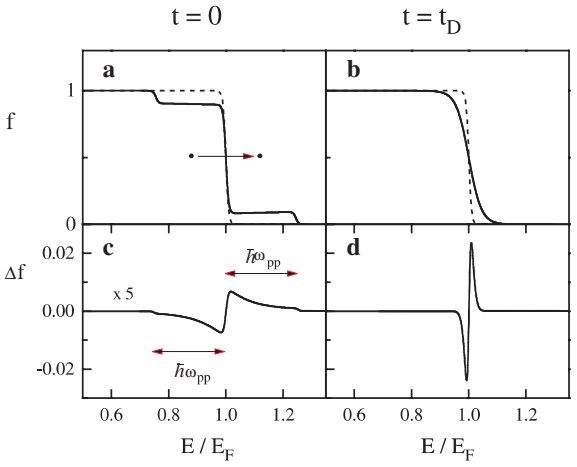

FIGURE 3 **a** Equilibrium (f_0, *dashed line*) and initial athermal (f, *solid line*) electron occupation number assuming instantaneous intraband excitation by a pump pulse of frequency $\omega_{\rm pp}$, with $\hbar\omega_{\rm pp} = 0.24E_{\rm F}$. **b** Same as **a** after establishment of an electron temperature (after a delay $t_{\rm D}$). **c** Δf computed at $t_{\rm D} = 0$ fs in Ag for $\Delta T_{\rm e}^{\rm me} = 100$ K and a 25 fs pump pulse at $\hbar\omega_{\rm pp} = 1.3$ eV. **d** Same as **c**, but for $t_{\rm D} = 1$ ps

1 ps. Δf initially extends over a very broad energy range and subsequently strongly narrows as the electron gas internally thermalizes. It has been shown that the electron relaxation dynamics is independent of the injected energy in the weak perturbation regime, i.e., for $\Delta T_{\rm e}^{\rm me} \leq 200$–$300$ K [16] ($\Delta T_{\rm e}^{\rm me}$ is defined as the temperature rise of a thermalized electron gas with the same excess energy as the total energy injected by the pump pulse). For larger energy injection, it depends on the excitation amplitude, with an acceleration of the internal thermalization of the electron gas [16] and a slowing down of its cooling [13–16].

Both the interband and intraband terms contribute to $\Delta\varepsilon$. The latter contribution is dominated by an increase in the electron optical scattering rate, $\gamma = 1/\tau$, and for a weak damping ($\omega^2\tau^2 \gg 1$), one can write

$$\begin{aligned} \Delta\varepsilon_1(\omega) &\approx \Delta\varepsilon_1^{\rm b}(\omega) \,, \\ \Delta\varepsilon_2(\omega) &\approx \Delta\varepsilon_2^{\rm b}(\omega) + (\omega_{\rm p}^2/\omega^3)\Delta\gamma(\omega) \,. \end{aligned} \tag{7}$$

Around the interband transition threshold $\hbar\Omega_{\rm ib}$, the interband absorption spectrum is determined by the occupation of the electronic states close to $E_{\rm F}$ and is thus modified by electron distribution smearing (Fig. 3) [23]. To quantitatively describe this effect, Rosei and co-workers modeled the bulk band structure of silver and gold around the Brillouin zone points contributing to the absorption [25, 26]. However, one has to keep in mind the fact that the Rosei models are valid for frequencies close to $\Omega_{\rm ib}$ and a thermalized electron gas. For strongly nonequilibrium electrons and a frequency away from $\Omega_{\rm ib}$, significant deviations can be observed and have to be taken into account to quantitatively compare the experimental and theoretical results [16]. In Ag, absorption takes place around the Brillouin zone L point, with a dominant contribution due to transitions from the d-bands to the conduction band ($d \rightarrow c$) and, a weaker one, due to transition from the conduction band to a higher energy empty s-band ($c \rightarrow s$). Using this model, in the constant transition matrix element approximation, $\Delta\varepsilon_2^{\rm b}$ can be related to Δf [25, 26]:

$$\Delta\varepsilon_2^{\mathrm{b}} \propto -\frac{1}{\omega^2}\left(\int_{E_{\mathrm{dc}}^{\mathrm{m}}}^{E_{\mathrm{dc}}^{\mathrm{M}}} D_{d\to c}(E,\omega)\Delta f(E)\mathrm{d}E - K_{\mathrm{sd}}\int_{E_{\mathrm{cs}}^{\mathrm{m}}}^{E_{\mathrm{cs}}^{\mathrm{M}}} D_{c\to s}(E,\omega)\Delta f(E)\mathrm{d}E\right), \quad (8)$$

where $D(E,\omega)$ is the energy-dependent joint density of state for the $c\to s$ or $d\to c$ transitions and $K_{\mathrm{sd}} = |P_{\mathrm{cs}}|^2 / |P_{\mathrm{dc}}|^2$ is their relative amplitude. $\Delta\varepsilon_1^{\mathrm{b}}$ is then obtained using the Kramers–Kronig relationship.

In this model, the width of the interband transitions has been neglected [8]. This is fully justified in the case of silver, for which we are interested in frequencies around the SPR, away from the interband transitions. For the same reason, the calculated $\Delta\varepsilon^{\mathrm{b}}$ is only weakly sensitive to the details of the band structure, and the simplified model of flat d-bands and parabolic conduction band leads to comparable results [12, 16].

In Au, only d-band to conduction band transitions take place, with a dominant contribution at the L point and a weaker one around the X point, at lower energy [26]:

$$\Delta\varepsilon_2^{\mathrm{b}} \propto -\frac{1}{\omega^2}\left(\int_{E_{\mathrm{dc,L}}^{\mathrm{m}}}^{E_{\mathrm{dc,L}}^{\mathrm{M}}} D_{d\to c}^{\mathrm{L}}(E,\omega)\Delta f(E)\mathrm{d}E + K_{\mathrm{XL}}\int_{E_{\mathrm{dc,X}}^{\mathrm{m}}}^{E_{\mathrm{dc,X}}^{\mathrm{M}}} D_{d\to c}^{\mathrm{X}}(E,\omega)\Delta f(E)\mathrm{d}E\right), \quad (9)$$

where K_{XL} is the relative amplitude of the $d\to c$ transitions at the X and L points. In contrast to silver, frequencies close to Ω_{ib} will be considered, making the results much more sensitive to the band structure modeling. Neglecting the interband transition width is also more questionable here. However, estimation of the actual influence of its change on $\Delta\varepsilon^{\mathrm{b}}$ is difficult, since its inclusion introduces an additional parameter when comparing experimental and theoretical results that could compensate for deviation between the real and model band structures. As a first approximation we have thus also not included it in the case of gold.

The $\Delta\varepsilon_1^{\mathrm{b}}$ and $\Delta\varepsilon_2^{\mathrm{b}}$ spectra computed for $t_{\mathrm{D}} = 0$ and 500 fs are shown in Figs. 1 and 2 for bulk silver and gold [16, 23]. Assuming that $\Delta\varepsilon^{\mathrm{b}}$ and its time evolution are identical in nanoparticles, the interband contribution $(\Delta T/T)_{\mathrm{b}}$ to $\Delta T/T$ is obtained using (6).

In silver, the computed $(\Delta T/T)_{\mathrm{b}}$ exhibits two distinct spectral features around Ω_{ib} and Ω_R with very different time behaviors (Fig. 1). The former is similar to that observed in bulk silver and corresponds to resonant probing of the interband transitions [16]. In this region, t_1 and t_2 are small and almost undispersed. The $(\Delta T/T)_{\mathrm{b}}$ spectral shape thus reflects the strong dispersion of the real and imaginary parts of $\Delta\varepsilon^{\mathrm{b}}$. Its time behavior is directly related to the electron distribution around the Fermi energy and thus to the internal electron thermalization dynamics. In particular it exhibits a delayed rise, the signature of the non-instantaneous establishment of an electron temperature [16, 27].

In contrast, the structure around Ω_R is a consequence of the well-known resonant enhancement of the nonlinear optical response around the SPR due to the dielectric confinement effect [3–5]. It is specific to confined systems and, in our approach, is reflected in a large amplitude and dispersion of t_1 and t_2 around Ω_R. In this region, $\Delta\varepsilon^{\mathrm{b}}$ is small and almost undispersed, since it corresponds to frequencies away from the interband transitions threshold. Actually, Ω_R being much smaller than Ω_{ib}, $\Delta\varepsilon_2^{\mathrm{b}}(\omega\approx\Omega_R)$ is nonzero only for very short times, t_{D}, when the conduction electrons are strongly out of equilibrium (typically for $t_{\mathrm{D}} \leq 50$ fs). The short time scale $\Delta\varepsilon_2^{\mathrm{b}}$ contribution shows up as a small red shift of the computed $(\Delta T/T)_{\mathrm{b}}$ spectral shape for $t_{\mathrm{D}} = 0$ fs, as compared to the ones for $t_{\mathrm{D}} = 100$ and 500 fs. For these longer delays, only $\Delta\varepsilon_1^{\mathrm{b}}$ is nonzero around $\hbar\Omega_R$ (optical Kerr effect) and the $(\Delta T/T)_{\mathrm{b}}$ spectral shape reflects that of t_1. Its time behavior essentially follows that of $\Delta\varepsilon_1^{\mathrm{b}}(\Omega_R)$, which has been shown to be almost identical to the time evolution of the electron gas excess energy [16, 28, 29]. Consequently, in this spectral range $(\Delta T/T)_{\mathrm{b}}$ "instantaneously" rises with energy injection in the electrons and decays with the electron energy losses to the lattice.

In gold, the SPR is close to Ω_{ib}, and these two features overlap, leading to more complicated spectral and temporal behaviors of $(\Delta T/T)_{\mathrm{b}}$ (Fig. 2). The spectral shape is actually determined by both the nonlinear enhancement effects (t_1 and t_2 dispersions) and the interband transition feature ($\Delta\varepsilon_1^{\mathrm{b}}$ and $\Delta\varepsilon_2^{\mathrm{b}}$ dispersions). This leads in particular to a small drift with time in the frequency where $(\Delta T/T)_{\mathrm{b}}$ is maximum, mostly due to the evolution of the $\Delta\varepsilon$ spectral shape during electron thermalization ($t_{\mathrm{D}} \leq 500$ fs [16, 23]). The time evolution of $(\Delta T/T)_{\mathrm{b}}$ is largely influenced by the internal electron thermalization, showing a delayed rise and frequency-dependent decays (see below). Similar effects are expected in copper, which exhibits the same degeneracy between the interband transitions and SPR [2, 7, 8].

The intraband contribution to $\Delta\varepsilon$ is due to the dependence of the probabilities of all the electron scattering processes on the electron distribution (or temperature T_{e} when it is established) and lattice temperature, T_{L}. In nanoparticles, we can write

$$\Delta\gamma = \Delta\gamma_{\text{e-ph}}(T_{\mathrm{e}}, T_{\mathrm{L}}) + \Delta\gamma_{\text{e-e}}(T_{\mathrm{e}}) + \Delta\gamma_{\mathrm{S}}(T_{\mathrm{e}}), \quad (10)$$

where $\gamma_{\mathrm{S}} = g_{\mathrm{S}}(T_{\mathrm{e}})V_{\mathrm{F}}/R$. Note that the T_{e} dependences of the electron optical scattering rates are however much weaker than for the DC ones, $\gamma(\omega = 0)$. The last term has been shown to yield an important contribution in small metal nanoparticles and is actually the manifestation of quantum confinement in their nonlinear optical response [6, 12].

The increase in the lattice temperature leads to an increase in the electron–phonon scattering rate, $\gamma_{\text{e-ph}}$, proportional to ΔT_{L} [6]. In the equilibrium regime ($T_{\mathrm{e}} = T_{\mathrm{L}}$), the purely electronic mechanisms are almost negligible (since $\Delta T_{\mathrm{L}} \ll \Delta T_{\mathrm{e}}^{\mathrm{me}}$), and $\Delta\gamma$ is essentially determined by ΔT_{L}. The electron–electron and electron–surface terms ($\Delta\gamma_{\text{e-e}}$ and $\Delta\gamma_{\mathrm{S}}$) rise and decay with the electron temperature, while $\Delta\gamma_{\text{e-ph}}$ rises with the lattice temperature (i.e., T_{e} decay). They

thus exhibit different time behaviors, leading to a weak overall time-dependence decay of the intraband part of $\Delta\varepsilon_2$ in films [29]. This detailed $\Delta\gamma$ time dependence will not be directly considered here, where we will only introduce $\Delta\gamma$ as a global parameter to compare the experimental and theoretical data.

It is interesting to note that in the case of silver, if the real and imaginary parts of $\Delta\varepsilon$ are weakly dispersed, the characteristic spectral shape of their contributions to $\Delta T/T$ imposed by the t_1 and t_2 dispersion closely corresponds to that obtained for a SPR spectral shift and broadening, respectively. This is simply related to the fact that in silver the SPR takes a quasi-Lorentzian shape with a frequency determined by $\varepsilon_1(\Omega_R)$ and a width determined by $\varepsilon_2(\Omega_R)$ [6, 12]. The full approach used here can thus be reduced to a simple analysis in terms of SPR frequency shift and induced broadening, related to $\Delta\varepsilon_1(\Omega_R)$ and $\Delta\varepsilon_2(\Omega_R)$ [6, 12]. This is not the case in gold, for which the linear absorption spectrum around the SPR cannot be simply described by a quasi-Lorentzian shape. In particular, although the lineshape of the computed $\Delta T/T_\mathrm{b}$ is similar to the one obtained for an induced broadening effect, it cannot be interpreted in term of SPR broadening, nor related to an electron scattering rate increase. Its physical origin is much more complex and is related to both $\Delta\varepsilon_1^\mathrm{b}$ and $\Delta\varepsilon_2^\mathrm{b}$, whose contributions are weighted by the enhancement of the nonlinear response around the SPR (Fig. 2).

4 Comparison with experimental results

The above electron kinetic and band structure model was developed for bulk materials. To a large extent, it is also applicable to not too small objects where the main band structure features of the bulk material are retained (at least for $R \geq 1.5$ nm), and the amplitude of the electron interaction processes are almost unchanged. This is the case for $R \geq 5$ nm silver and gold nanoparticles that have been shown to exhibit bulk-like electron kinetics [27, 30], and we will focus here on these relatively large nanoparticles.

4.1 Ag *case*

The spectral shape of the normalized transient transmission $\Delta T/T$ measured around the SPR ($\hbar\Omega_R = 2.93$ eV) in $R = 13$ nm silver nanoparticles in glass is shown in Fig. 4 for a fixed pump–probe delay, $t_\mathrm{D} = 1$ ps. The results were obtained in the weak perturbation regime ($\Delta T_\mathrm{e}^\mathrm{me} \approx 150$ K) using a 25 fs near-infrared pump pulse and a 30 fs probe pulse [12]. A similar derivative type of shape has been observed for all the investigated samples, with mean radii ranging from 2 to 15 nm, and positive time delays. It is comparable to the computed $(\Delta T/T)_\mathrm{b}$, i.e., taking into account only the change of the interband part of ε (Fig. 1). For this time delay, only $\Delta\varepsilon_1^\mathrm{b}$ contribute to $(\Delta T/T)_\mathrm{b}$. Introduction of a nonzero $\Delta\varepsilon_2$ leads to the same type of shape, but red shifts the $\Delta T/T$ spectra and increases its asymmetry.

Quantitatively comparing the measured $\Delta T/T$ and computed $(\Delta T/T)_\mathrm{b}$, both the asymmetry of the experimental spectra and the frequency where it changes sign cannot be reproduced (Fig. 4). The same type of discrepancy has been observed for all the studied time delays and nanoparticle sizes [6, 12]. This is ascribed to the contribution of the intraband term to $\Delta\varepsilon$ (7), i.e., to the induced increase in the electron scattering rate. A fairly good reproduction of the experimental data is obtained by adding an intraband contribution, using the $\Delta\gamma$ amplitude as a parameter (Fig. 4). This is equivalent to introducing a broadening of the SPR, as done using the simplified modeling in terms of modification of the SPR lineshape. Similar agreements have been obtained over the investigated time delay and nanoparticle size ranges. It has been shown that this contribution, and consequently the observed deviation, is larger for small nanoparticles and short time delays due to the increasing contribution of $\Delta\gamma_\mathrm{S}$ with size reduction [12].

To further analyze the different contributions to $\Delta\varepsilon$, it is interesting to compare the time-dependent measured and computed data at a fixed probe frequency around Ω_R (Fig. 5). A very good reproduction of the measured time behavior is obtained, with in particular the same short time delay transient for probing at the SPR ($\hbar\omega_\mathrm{pr} = \hbar\Omega_R = 2.93$ eV). This actually reflects the transient contribution of $\Delta\varepsilon_2^\mathrm{b}$ and is thus the manifestation of the noninstantaneous electron thermalization, i.e., of the transient athermal character of the electron distribution in the nonlinear response. The relaxation of the involved electron states far from E_F is very fast (few fs), and thus this feature can only be observed using short pulses. It is almost washed out for a pulse duration of $t_\mathrm{p} \geq 50$ fs, the athermal character of the distribution leading then to only weak modifications of the measured response.

On a longer time scale ($t_\mathrm{D} \geq 150$ fs), the calculated decay is similar for different probe wavelengths, as shown in Fig. 6 for $\hbar\omega_\mathrm{pr} = \hbar\Omega_R$ and $\hbar\omega_\mathrm{pr} = \hbar\Omega_R \pm 50$ meV (only

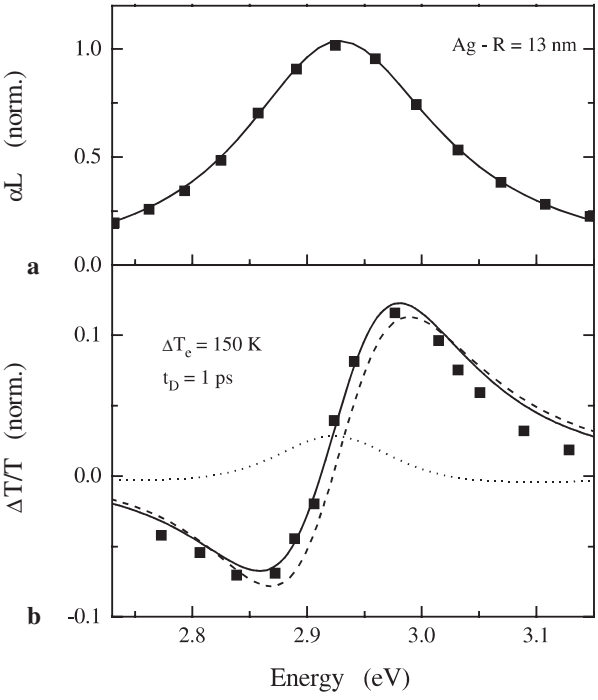

FIGURE 4 **a** Measured (*squares*) and computed (*solid line*, see Fig. 1) absorption spectrum of $R = 13$ nm silver nanoparticles in glass. **b** Measured spectrum of the transmission change around the SPR in the same sample for a pump–probe delay of $t_\mathrm{D} = 1$ ps (*squares*). The *dashed line* is the calculated $\Delta T/T$, for only the interband contribution ($(\Delta T/T)_\mathrm{b}$, Fig. 1), and the *dotted line* is the intraband contribution [due to $\Delta\gamma$ in (7)]. The *solid line* is their sum

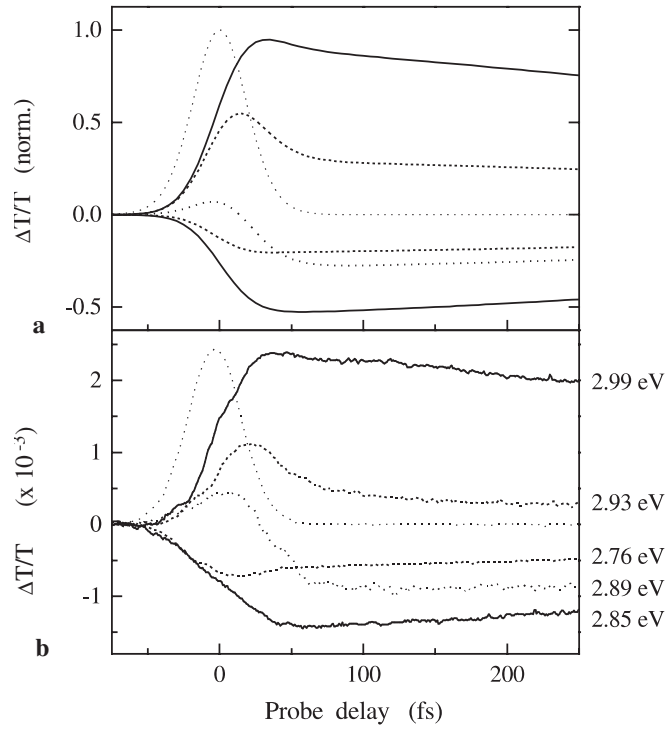

FIGURE 5 **a** Calculated and **b** measured time dependences of the normalized transmission change in $R = 13$ nm silver nanoparticles in glass for the different probe photon energies indicated in **b**, around the SPR frequency ($\hbar\Omega_R = 2.93$ eV) for $\Delta T_e^{me} = 150$ K. The duration of the infrared pump pulse is 25 fs and that of the probe pulse 30 fs. The *thin dotted lines* are the pump–probe cross correlations

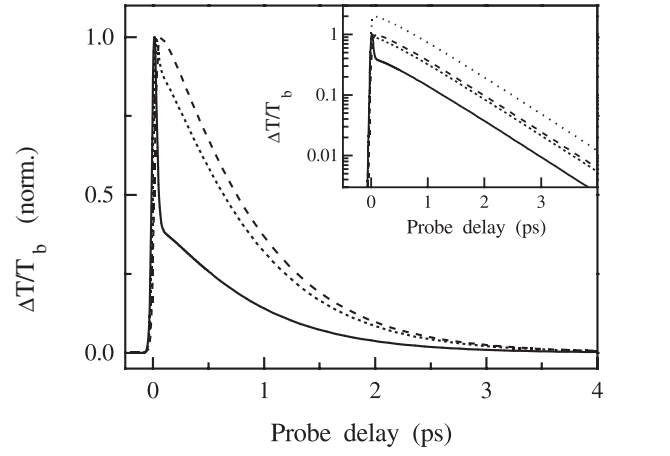

FIGURE 6 Calculated picosecond time scale dependence of $\Delta T/T$ in $R = 13$ nm silver nanoparticles in glass for different probe photon energies $\hbar\omega_{pr} = \hbar\Omega_R$ (*solid line*), $\hbar\Omega_R + 50$ meV (*short-dashed line*) and $\hbar\Omega_R - 50$ meV (*dashed line*). The excitation and probing condition are the same as in Fig. 5. The inset shows the same data on a logarithmic scale, together with the time evolution of the excess energy stored in the electron gas (*dotted line*, vertically shifted for clarity)

$(\Delta T/T)_b$ has been considered here). This is more clearly observed by plotting the time-dependent $(\Delta T/T)_b$ on a logarithmic scale, the same type of decay being observed after 50–100 fs, with, in particular, an exponential behavior after typically 500–700 fs. The delay in reaching an exponential evolution is a consequence of the athermal character of the electron distribution and has been discussed in Ag films elsewhere [29]. As expected, the time evolution is almost identical to the one of the excess energy stored in the electron gas. Similar results were obtained in the strong excitation regime ($\Delta T_e^{me} = 1000$ K), with a lengthening of the computed decay due to the temperature dependence of the electron heat capacity. These results are in agreement with the experimental ones, showing, in particular, no wavelength dependence of the measured decay rate [6, 12].

4.2 Au *case*

The transient responses of gold nanoparticle samples have been investigated mostly in the strong excitation regime [9–11, 14, 15]. Extending our simulation to this regime, the calculated transient $(\Delta T/T)_b$ lineshapes were found to be very similar to the ones shown in Fig. 2 in qualitative agreement with the measured ones. The $(\Delta T/T)_b$ spectrum computed for $R = 15$ nm gold nanoparticles for $\Delta T_e^{me} = 3700$ K and $t_D = 1.5$ ps is compared to the experimental one measured by M. Perner et al. in Fig. 7 [10]. A good description of the experimental data is obtained, with, in particular, the same spectrum asymmetry. Note that no parameter has been used here.

These results confirm that the interband term dominates the nonlinear response and indicate a weak influence of the electron scattering rate increase (i.e., of the intraband term) in gold [11, 15, 31]. This is consistent with the results in silver, for which the latter contribution has to be taken into account only because of the weak amplitude of $\Delta\varepsilon^b$ far from the interband transition threshold. This is not the case in gold, for which $\Delta\varepsilon^b$ is large around the SPR frequency.

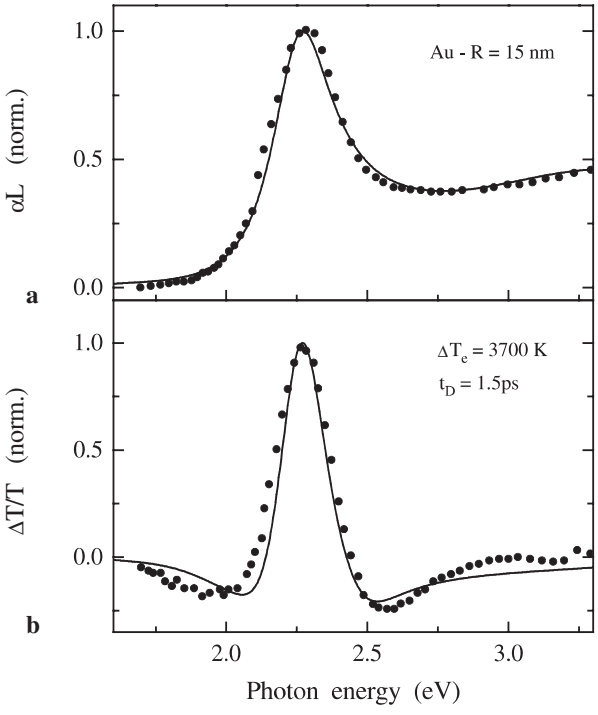

FIGURE 7 **a** Measured absorption spectrum of $R = 15$ nm gold nanoparticles in a sol–gel film (*circles*, from [10]). The *solid line* is the computed spectrum. **b** Measured spectrum of the transmission change around the SPR in the same sample for a pump–probe delay of $t_D = 1.5$ ps (*circles*, from [10]). The *solid line* is the calculated $\Delta T/T$, taking into account only the interband contribution $(\Delta T/T)_b$ for the same excitation condition ($\Delta T_e^{me} = 3700$ K)

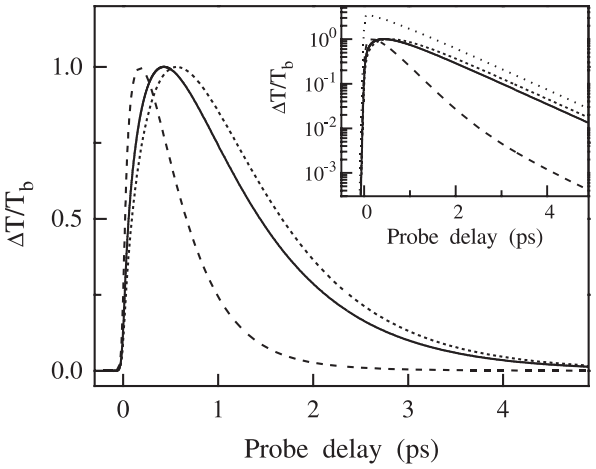

FIGURE 8 Calculated time dependence of $\Delta T/T$ in $R = 5$ nm gold colloid for different probe photon energies, $\hbar\omega_{\rm pr} = \hbar\Omega_{\rm R}$ (*solid line*), $\hbar\Omega_{\rm R} + 50$ meV (*short-dashed line*) and $\hbar\Omega_{\rm R} - 50$ meV (*dashed line*), and $\Delta T_{\rm e}^{\rm me} = 150$ K. The duration of the infrared pump pulse is 25 fs and that of the probe pulse 30 fs. The inset shows the same data on a logarithmic scale, together with the time evolution of the excess energy stored in the electron gas (*dotted line*, vertically shifted for clarity)

The measured lineshape is, however, slightly broader than the computed one. This discrepancy can be ascribed to different factors, such as oversimplification of the band structure by the Rosei's model or neglect of the increase in the width of the interband transitions [8]. Quantitative description of the data by adding the latter effect is difficult, since, as discussed above, the spectral shape of the computed response is very sensitive to the band structure model. It is, however, the most likely effect, a similar discrepancy having been observed in CW thermomodulation measurements and femtosecond investigations of gold films [23, 26].

In contrast to that for silver, the response around the SPR is strongly influenced by the athermal character of the distribution, and, in particular, exhibits a delayed rise-time, as observed experimentally [15]. The same effect has also been observed in copper [7, 8], which is expected to exhibit the same type of transient behavior. This delayed rise reflects the build-up of the electron distribution change around the Fermi energy during electron thermalization [16, 23]. As in metal film in the same frequency range, it leads to a strong frequency dependence of the $\Delta T/T$ time behavior [23], as shown in Fig. 8, for $\hbar\omega_{\rm pr} = \hbar\Omega_R$ and $\hbar\omega_{\rm pr} = \hbar\Omega_R \pm 50$ meV in the case of 5 nm gold colloid in the weak perturbation regime (similar dependences were computed for strong excitation, with, as for silver, a lengthening of the $\Delta T/T$ decay). This is due to the fact that the observed decays are not simply related to electron energy losses to the lattice, which globally describes the electron gas, but are also sensitive to the details of the occupation of the states around the Fermi energy.

5 Conclusion

The ultrafast optical nonlinearities in metal nanoparticles are related to the electron distribution change induced by the optical pulses, with negligible contribution from saturation effects. This is strongly enhanced by the dielectric confinement in the vicinity of the SPR, leading to the well-known SPR optical nonlinearity enhancement. A change in the electron distribution leads to modification of both the interband absorption spectrum, due to Fermi surface smearing, and the electron optical scattering rate, due to weakening of the Pauli exclusion principle effect. These reflect in the alteration of the interband and intraband parts of the metal dielectric function, respectively. These two effects play different roles, depending on the spectral position of the SPR as compared to the interband transition threshold.

Both effects contribute in the case of silver, where the SPR is well separated from the interband transitions. The induced changes of the real and imaginary parts of the metal dielectric function ($\Delta\varepsilon_1$ and $\Delta\varepsilon_2$) can then be interpreted in terms of SPR frequency shift and broadening, respectively, the observed spectral shapes being essentially related to the SPR effect. The real part of the interband term always dominates the SPR shift. In contrast, the imaginary part of the interband term only contributes on a very short time scale when the electron gas is strongly athermal (≤ 50 fs). The intraband one dominates the longer time scale with an important contribution due to an increase in the electron–surface optical scattering rate with heating of the electron gas. This mechanism is specific to confined systems and is a manifestation of quantum confinement in the nonlinear optical response.

In contrast to silver, the SPR overlaps the interband transitions in gold nanoparticles, and both the real and imaginary parts of the interband term contribute and dominate their nonlinear response for any time delay. Their simultaneous contributions, weighted by the SPR-related enhancement of the nonlinearity, are at the origin of the observed transmission change spectral shape, which cannot be related to a simple change in the SPR lineshape. This overlap also leads to a frequency-dependent relaxation of the optical nonlinearity, as observed in metal film. Similar behaviors are expected in copper nanoparticles, which exhibit the same SPR–interband transition degeneracy.

Although a good reproduction of the spectral and time dependence of the experimental nonlinear responses is obtained, one has to keep in mind the fact that the bulk material electron kinetics and band structures have been used. This approach is valid for the not too small nanoparticles ($R \geq 5$ nm) considered here, whose spectral and dynamic properties are known to be close to the bulk ones, but overlooks specific features of the electron dynamics in confined systems, such as the size dependence of the electron scattering rates [27, 30]. These have to be included in models of the ultrafast nonlinearities of smaller size nanoparticles.

REFERENCES

1 A. Kawabata, R. Kubo: J. Phys. Soc. Jpn. **21**, 1765 (1966)
2 U. Kreibig, M. Vollmer: *Optical Properties of Metal Clusters* (Springer, Berlin 1995)
3 C. Flytzanis, F. Hache, M.C. Klein, D. Ricard, P. Roussignol: In *Progress in Optics*, Vol. XXIX, ed. by E. Wold (North-Holland, Amsterdam 1991) p. 321
4 D. Ricard: In *Nonlinear Optical Materials: Principles and Applications*, ed. by V. Degiorgio, C. Flytzanis (IOS Press, Amsterdam 1995) p. 289
5 R.F. Haglund: In *Handbook of Optical Properties*, Vol. 2, ed. by R.E. Hummel, P. Wissmann (CRC Press, New York 1997) p. 191
6 C. Voisin, N. Del Fatti, D. Christofilos, F. Vallée: J. Phys. Chem. B **105**, 2264 (2001)

7 T. Tokizaki, A. Nakamura, S. Kavelo, K. Uchida, S. Omi, H. Tanji, Y. Asahara: Appl. Phys. Lett. **65**, 941 (1994)
8 J.Y. Bigot, J.C. Merle, O. Cregut, A. Daunois: Phys. Rev. Lett. **75**, 4702 (1995)
9 J.Z. Zhang: Acc. Chem. Res. **30**, 423 (1997) and references therein
10 M. Perner, P. Bost, U. Lemmer, G. von Plessen, J. Feldmann, U. Becker, M. Mennig, M. Schmitt, H. Schmidt: Phys. Rev. Lett. **78**, 2192 (1997)
11 H. Inouye, K. Tanaka, I. Tanahashi, K. Hirao: Phys. Rev. B **57**, 11 334 (1998)
12 N. Del Fatti, F. Vallée, C. Flytzanis, Y. Hamanaka, A. Nakamura: Chem. Phys. **215**, 251 (2000)
13 Y. Hamanaka, A. Nakamura, S. Omi, N. Del Fatti, F. Vallée, C. Flytzanis: Appl. Phys. Lett. **75**, 1712 (1999)
14 J.H. Hodak, I. Martini, G.V. Hartland: J. Phys. Chem. B **102**, 6958 (1998)
15 S. Link, M.A. El-Sayed: J. Phys. Chem. B **103**, 8410 (1999)
16 N. Del Fatti, C. Voisin, M. Achermann, S. Tzortzakis, D. Christofilos, F. Vallée: Phys. Rev. B **61**, 16 956 (2000)
17 P.B. Johnson, R.W. Christy: Phys. Rev. B **6**, 4370 (1972)
18 H. Ehrenreich, H.R. Philipp: Phys. Rev. **128**, 1622 (1962)
19 F. Hache, D. Ricard, C. Flytzanis: J. Opt. Soc. Am. B **3**, 1647 (1986)
20 H. Hovel, S. Fritz, A. Hilger, U. Kreibig, M. Vollmer: Phys. Rev. B **48**, 18 178 (1993)
21 A. Knoesel, A. Hotzel, M. Wolf: Phys. Rev. B **57**, 12812 (1998)
22 R. Matzdorf, A. Gerlach, F. Theilmann, G. Meister, A. Goldmann: Appl. Phys. B **68**, 393 (1999)
23 C.K. Sun, F. Vallée, L.H. Acioli, E.P. Ippen, J.G. Fujimoto: Phys. Rev. B **50**, 15 337 (1994)
24 C. Voisin, D. Christofilos, N. Del Fatti, F. Vallée: Eur. Phys. J. D, to be published
25 R. Rosei: Phys. Rev. B **10**, 474 (1974)
26 R. Rosei, F. Antonangeli, U.M. Grassano: Surf. Sci. **37**, 689 (1973)
27 C. Voisin, D. Christofilos, N. Del Fatti, F. Vallée, B. Prével, E. Cottancin, J. Lermé, M. Pellarin, M. Broyer: Phys. Rev. Lett. **85**, 2200 (2000)
28 R. Groeneveld, R. Sprik, A. Lagendijk: Phys. Rev. B **51**, 11 433 (1995)
29 N. Del Fatti, R. Bouffanais, F. Vallée, C. Flytzanis: Phys. Rev. Lett. **81**, 922 (1998)
30 N. Del Fatti, C. Flytzanis, F. Vallée: Appl. Phys. B **68**, 433 (1999)
31 G.V. Hartland, J.H. Hodak, I. Martini: Phys. Rev. Lett. **82**, 3188 (1999)